

Novel Derivations & Validations of Near-field Electromagnetic Spatial Power Density Distribution and Propagation Functions for Flat Antennas

by

M. Nisa Khan, SENIOR MEMBER, IEEE

IEM LED Lighting Technologies,
Red Bank, NJ 07701, USA
email: nisa.khan@IEM-LED.com

Published February, 17, 2022

PRINCIPIA
SCIENTIFIC



International

See Principia-scientific.org under
'SUPPORT/NEWS' 'HOW THE PROM PROCESSWORKS'

Novel Derivations and Validation of Near-field Electromagnetic Spatial Power Density Distribution and Propagation Functions for Flat Antennas

M. Nisa Khan, Senior Member, IEEE

IEM LED Lighting Technologies, 331 Newman Springs Road, Red Bank, NJ 07701 USA

Email: nisa.khan@IEM-LED.com

Abstract: We derive novel closed-form analytic functions for the near-field electromagnetic (EM) spatial power density distributions for flat or patch antennas. The derived functions enable us to analytically describe how the EM field flux generated from such antennas propagates in space, allowing us to quantify the radiation power density at any point in space. Such calculation abilities have been lacking in the industry since the inception of wireless communication dating back for over a century. Our derivations are based on how radiation sources inherently generate EM field flux in space based on Gauss' Law and Maxwell's Equations, which are also used to derive the Helmholtz wave equation. We validate our near-field analytic functions for a flat antenna using a commercial EM simulation software tool. Our novel solutions offer a unique and rapid method for calculating the peak and minimum spatial power densities of wireless signals anywhere in space, which are very important parameters for designing mm-Wave wireless systems including 5G networks. Our derived functions offer new methods for calculating and simulating the near-field power gain functions of patch antennas that can be used to calculate the far-field gain function in a more straightforward manner than the practice currently used by all RF simulation techniques.

Index Terms: Electromagnetics, closed-form analytic solutions, fifth generation (5G), Maxwell's Equations, mm-Wave, propagation.

1. Introduction

The utilization of wireless or radio communication systems has been continuously expanding for various levels of personal, commercial, and governmental applications. Higher and higher degree of mobile usage is enabled with increasing data speed and bandwidth (i.e., spectrum) in wireless systems. Currently, the fifth generation (5G) wireless technology is being pursued aggressively to support a very large amount of fast data transfers that provide continuous and ubiquitous use of video and Internet of Things (IoT). Such 5G systems invariably make use of millimeter wave (mm-Wave) frequencies that allow information exchange at multi-Gigabit-per-second (Gbps) data rates among mobile devices, which are also referred to as user equipment (UE) [1]. As data rates and the number of UE's increase substantially, signal power requirements also increase and therefore the need for accurate prediction of required signal power becomes crucial.

Wireless signals operating at high carrier and modulation frequencies are restricted in the distance they travel because the signals lose fidelity beyond certain limit. For example, Ghosh et al. and Roh et al. showed utilizing 4X4 phased array antennas that personal mobile devices can operate at 15 Gbps peak rates only within the maximum spacing between base stations of 200m [2], [3]. Thus we expect distances between base stations in living areas to be fairly short in order for the

public to have access to 5G cellular networks. While reducing distances can make 5G or 6G networks feasible, designing antennas for optimal power can provide better flexibility for wireless network design. The derived spatial power distribution formulas presented in this paper offers new methods to design antennas for optimal power output.

Commercial wireless antennas are known to have spatial directivity and as such one would expect signals generated from a base station via a single antenna unit to have coverage within only a limited angular distribution. In order to cover a living area within a certain kilometer radius all around a base station, several antenna units are typically used pointing in different directions to cover different conical zones as seen in Fig.1. The wireless signal power densities within a conical zone from a single antenna unit are spatially non-uniform and as such, base stations are generally designed to provide certain minimum signal strength i.e., a minimum EM power density measure that is required for UE's to operate within this conical zone from each directive antenna. Such designs use various numeric models and approximation techniques to determine how wireless signals propagate in space [4], [5], [6].



Figure 1. Directional antenna units are pointed at various directions around the pole to provide radial coverage in a specified living area.

In this paper, we derive a novel, closed-form analytic function for the 3D near-field spatial power density distribution for a flat antenna of certain size. From this function, we derive the surface power density distribution that is directly proportional to the surface flux field, by taking the 3D function's projection onto the 2D antenna surface. Our closed-form analytic function for the surface power density distribution enables us to write the analytic equation for how antenna waves propagate in space. These formulas offer a unique way of calculating the peak and the minimum power densities of mm-Wave wireless signals, generated from flat antenna structures, at specific locations. Both peak and minimum power density quantities are very important for designing a consumer 5G wireless network because lacking such knowledge will lead to grossly excessive RF power densities in space.

We have previously published similarly derived near-field radiant intensity functions for a flat optical radiation source [7] utilizing Lambert's Cosine Law [8]. However, the derivation presented in this paper does not assume Lambert's Cosine Law to arrive at the 3D near-field radiant intensity

function for a radiator emitting EM wave. Instead, in this paper, we start our derivation from Maxwell's Equations for electrodynamics while applying Gauss' Divergence Theorem for a finite, flat radiation source. Maxwell's Equations and Gauss' Divergence Theorem are the very fundamentals that describe electromagnetic radiation behaviors and mathematical manipulation of these theories lead to the fundamental wave equation, i.e., the Helmholtz wave equation. In general, this wave equation is solved for any arbitrary radiation source structure to determine how it generates EM waves, which encompass both optical and RF fields. Our paper proves for the first time that Lambert's Law is consistent with Maxwell's Equations and Gauss' Law, which is significant because Lambert's Law existed for light radiation well before Maxwell's Equations were discovered in the nineteenth century. This is similarly interesting as when scientists of latter times proved that Snell's Law is also consistent with Maxwell's Equations. Such scientific and mathematical consistencies are both important and intriguing for the field of physics and electrical engineering.

2. Derivation of the 3D Near-field Power Density Distribution from a Flat Antenna

Wireless signal strength at a location is quantified by means of the power density (W/m^2) of the electromagnetic radiation (EMR) of certain frequency at that location that contains coded data transmitted from a source antenna (base station) certain distance away. The electromagnetic radiation comprises of the frequency spectrum chosen by the carrier; the spectrum is defined by the EMR power distribution within this frequency band. Carriers utilize a number of frequencies from this band as separate channels and each such channel contains its own data signals of different modulation frequencies. Determining the signal strength at certain distance from the base station has largely become a statistical modeling problem based on propagation measurements and models [9], [10], [11] due to statistical distribution effects arising from bandwidth and data-speed dependencies, rapid movements of signal waves through the scattering environment, impairments due to long echoes leading to inter-symbol-interference and other signal characteristics and quality issues. However, these methods cannot accurately determine the EMR **spatial** power density variation with sufficient resolution. Here we find a closed-form analytic solution for the basic EMR spatial power density distribution generated by a base station antenna over a certain area or volumetric zone of interest as this is the basic requirement for achieving reliable communication. We separate our problem from that of temporal domain including the expected signal power fluctuation in time, and degradation or error issues that can be addressed using equalization, modulation, and coding schemes for a particular frequency channel. Although certain finite, numeric methods can approximate the spatial power density distributions, these do not include calculation of the peak, average, and minimum intensities at all locations in space from a finite, patch antenna and their arrays, with certain physical size, input drive conditions and inherent quantum efficiency, without resorting to some laborious brute-force and iterative techniques. In contrast, our derived analytical formula for a single patch antenna allows one to determine the full-vectorial spatial power density distribution in space based on the patch antenna's physical size, inherent quantum efficiency, and RF driving conditions.

We start with specifying the parameters of our focus in the classic electromagnetic signal equation in order to confine our problem in only the spatial domain. The electromagnetic wave that carries a radio signal can be written as [12],

$$E(x, y, z, t) = \Psi_0(x, y, z) e^{-j\omega t} e^{\pm j\vec{k} \cdot \vec{\rho}} \quad (1)$$

where E is the electric field flux distribution, Ψ_0 is the distribution of the electric field flux at $z = 0$, \vec{k} is the wavevector that relates to the medium permittivity and permeability, and $\vec{\rho}$ is the arbitrary direction that the electromagnetic wave propagates towards. The term $e^{-j\omega t}$ contains all temporal frequency and time dependent signal generation information and the power in that signal at any point in space and time is specified by EE^* or $|E|^2$. As a reminder, $e^{-j\omega t}$ part of the signal oscillates in time and $e^{\pm j\vec{k} \cdot \vec{\rho}}$ part of the signal oscillates in space. In this paper, the space oscillation term is our focus as we derive the spatial power density distribution, Ψ_0 , and therefore do not carry the term $e^{-j\omega t}$. This time-dependent term can be added in the same manner as shown in Eq.(1) when the total field at any given time and space needs to be determined.

The goal of this paper is to find Ψ_0 , which is the solution to the Helmholtz wave equation [12] that must be solved for an antenna generating the EMR. By definition, Ψ_0 is the near-field electric field flux distribution right off the antenna at time $t = 0$. The wave equation for a finite-size flat aperture or a patch antenna can be solved using finite element or finite difference numerical methods, which can incorporate time-domain terms when desired. In practice, most 5G antennas are an array of patches over a 2D plane and these also can be simulated using finite, numeric methods. But here we start with a novel approach, which makes use of the same basic physical laws that give rise to the wave equation [12] and we proceed to determine an analytic function for the 3D spatial distribution of the EMR produced by a single flat, patch antenna. To do such, we first assume that the antenna is a thin, flat electrode or conducting structure made up of many infinitesimally small radiative elements, (i.e. small dipole antennas) arranged over its flat area as shown in Fig. 2. There are two cases for solving this category of problem: 1) the coherent case where all radiative elements add in phase and 2) the incoherent case where all elements have random phase.

Here we first consider the latter case, which is the simpler of the two and has higher practical relevance. Our derivation can be extended for a 2D array of patch antennas by adding the solution of each patch antenna along with its neighbor patch antennas appropriately translated over a flat plane in much the same way the numerical methods do.

In the active part of the antenna structure, we assume that the radiative elements, on average, are arranged uniformly in a 2D array and each element is driven equally by a current source, without requiring the elements to be coherent. We therefore have a radiative, incoherent antenna that generates EMR due to spontaneous radiation emission, which is a quantum statistical process that happens very fast, i.e., at some microsecond level. Therefore when a steady current is uniformly injected into the antenna patch using a voltage or current signal, it generates radiation in a continuous manner. The spatial distribution of the small radiative elements in this active antenna patch is uniform on a time-averaged scale. In practice, in some cases, the radiative elements' spatial density distribution may not be uniform due to non-ideal material and drive conditions. For the case of non-uniform material, one can apply some weighted variation based on certain mapping

measurements of radiative elements' locations and distributions, and the formulation presented below can still be carried out by sequentially adding EMR generated from many different regions that have locally uniform radiative elements. For the case of non-ideal drive condition, one can achieve a semi-uniform current distribution by utilizing an adiabatic waveguide or transmission line feed to the patch with matching impedance.

Following the assumption that all radiative elements, dA 's, are arranged in a regular 2D array, we can think of each having an inherent radiance of R_{avg} as shown in Fig.2. Although in practice, many single antenna structures are typically square with the same x and y lengths, here we consider the patch antenna to be a rectangle to maintain a higher generality, with different x and y dimensional lengths, X_L and Y_L respectively, with a total of $m \times n$ radiative elements arranged in a 2D grid.

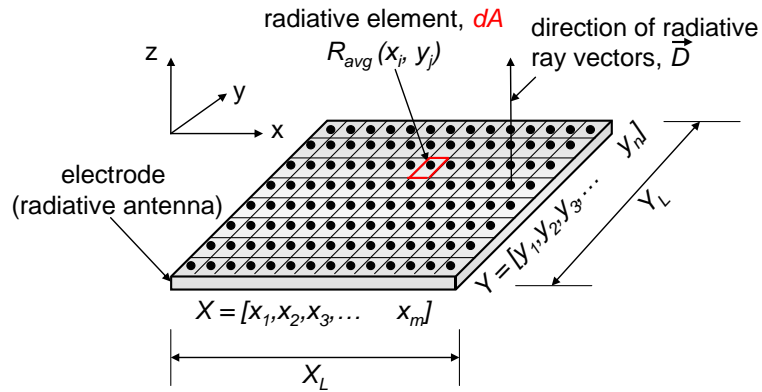


Figure 2. A schematic diagram of a flat, rectangular antenna containing $m \times n$ infinitesimally small radiative elements, or dA 's.

It is very well known that all 4 Maxwell's Equations along with Gauss' Divergence Theorem are utilized to describe how a radiator emits radiation in space or any media as well as time and how such radiation is propagated through space. Two of the 4 Maxwell's Equations use the divergence of electric and magnetic fields via the 'del' operator and these are known as Gauss' Law of electric and magnetic fields. The 'del' operator is time independent and when it is applied to the electric and magnetic fields as a dot product, the results do not generate any time-dependent behavior and therefore many mistake these two Maxwell's Equations to be only true for electrostatics and magnetostatics. This is indeed a grave mistake because the 'del' operator is merely a spatial derivative and thus their divergence only describes spatial characteristics of the electric and magnetic fields and these need not have any time-varying properties to play their role in electrodynamics. Electrodynamics fully describes both temporal and spatial characteristics simultaneously and for such, all 4 Maxwell's Equations must be utilized simultaneously as done in deriving the classic Helmholtz wave equation [12]. Here we employ Maxwell's Equations for

polarizable dielectric materials [13] in order to determine how EMR escapes the antenna's structural solid in Fig.2. Since each small antenna element, dA , on the surface of the patch can emit radiation, it would do so following the first of the 4 Maxwell's Equations known as the Gauss' Law or Gauss' flux theorem for polarizable dielectric materials [13] given by

$$\oiint_S \vec{D} \cdot d\vec{A} = \Phi_D = Q_{free} \quad (2)$$

where Φ_D is the D-field flux through a surface element S , which encloses a volume V , and Q_{free} is the total free charge contained in V . The free charges are those that are allowed to escape the solid.

The flux Φ_D is defined analogously to the flux Φ_E of the electric field \vec{E} through S . Eq.(2) in detailed form can be written as

$$\oiint_S \vec{D} \cdot d\vec{A} = \Phi_D = \int_V \rho_{free}(V) dV = Q_{free} \quad (3)$$

Using the Divergence Theorem as done in [14],

$$\iint_S \vec{F} \cdot \vec{n} dS = \iiint_V \vec{\nabla} \cdot \vec{F} dV \quad (4)$$

we can write Eq.(2), Gauss's Law, in its differential form involving free charge only:

$$\vec{\nabla} \cdot \vec{D} = Q_{free} \quad (5)$$

where $\vec{\nabla} \cdot \vec{D}$ is the divergence of the electric displacement field \vec{D} , and ρ_{free} is the free electric charge density.

The Divergence Theorem in Eq.(4) allows one to write Gauss' Law in integral and differential form; and Eqs.(2) through (5) together dictate the radiation escape direction from each radiative element dA . The Divergence Theorem dictates that based on the spatial characteristics of the solid that encloses the electrically charged elements within a bounded volume of the solid, each \vec{D} for each surface element escapes normal to that surface element as dictated by the dot products present in both sides of Eq.(4).

The usage of Maxwell's Equation for the divergence of \vec{D} and the usage of the Divergence Theorem under these circumstances form the basis of EMR flux emission from antennas [13]. In homogeneous, isotropic, nondispersive, linear materials, the simple relationship between \vec{E} and \vec{D} is $\vec{D} = \epsilon \vec{E}$ [13] where ϵ is the permittivity of the material. For the case of vacuum (i.e., free space), $\epsilon = \epsilon_0$. Under these circumstances, Gauss' Law modifies to the simpler versions [13],

$$\oiint_S \vec{E} \cdot d\vec{A} = \Phi_E = \frac{Q}{\epsilon_0} \quad \text{and} \quad \vec{\nabla} \cdot \vec{E} = \frac{\rho}{\epsilon_0}.$$

Note that in the above equation, ρ represents charge inside the radiation source and it should not be confused with the spatial vector $\vec{\rho}$ used in Eq.(1) and in the following analyses where $\vec{\rho}$ is a variable in the spherical coordinate system. From the analysis above, it follows that all radiated

rays specified by the electric field displacement vector, \vec{D} in Eq.(6) from each differential flat antenna element, dA , escape the flat surface orthogonal or normal to the flat surface, dA .

The radiation intensity, I , is obtained from $I \propto \vec{E} \cdot \vec{E}^*$ or $I = |\vec{E}|^2$ which can also be calculated from the Poynting vector, \vec{S} , where $\vec{S} = \vec{E} \times \vec{H}$ since E and H are both related in space (generally considered non-magnetic) by means of the 4 Maxwell's Equations. It is important to note that in vacuum and in non-magnetic media, \vec{E} (or \vec{D} with a scaling factor) is the same as the magnetic field, \vec{B} (or \vec{H} with a scaling factor). Numeric methods, such as finite element waveguide antenna and beam propagation simulation tools also make use of this formula to determine radiation intensity in various media including solids.

The above analysis establishes that from each differential element, dA , from the emitting surface in Fig.2 emits a radiative ray, \vec{D} (the displacement field of \vec{E}) orthogonal to dA . If any coatings are fabricated on this surface as a parallel layer, radiative rays through the coating would escape similarly as \vec{D} from the original radiative element, i.e., orthogonally from each flat differential element, dA . In other words, the emitted radiative ray would maintain its orthogonal directivity even through the coating layer. This behavior is dictated by the electromagnetic boundary condition, which states that normal \vec{D} must be continuous through all dielectric boundaries [13]. This boundary condition is fundamental to finite element and finite difference waveguide and beam propagation simulation tools that are used to determine radiation emission and propagation in various media. It is important to note that while \vec{D} and \vec{E} are vectors that represent directive radiative rays associated with each dA , the flux or radiation they generate in space is not a vector; but rather flux or radiation has a spatial distribution. Radiation intensity distribution is directly proportional to this flux distribution.

A good portion of the analysis and explanation presented above has been extensively used in prior academic literature for many years [12] [13]. It is presented in full detail here in order to clarify many common misunderstandings between flux that is a scalar quantity and a single directed vector field, \vec{D} or \vec{E} that represents the direction at which radiation escapes its source's infinitesimal surface. Furthermore, we have also highlighted the notable addition that \vec{D} specifically escapes orthogonally from a flat antenna source surface no matter how many additional parallel layers are placed on top of the original patch antenna. This behavior is consistent for an infinitesimally small flat radiation source, which we demonstrate below by making use of the very the definition of radiant intensity, which is proportional to flux density.

It is well-known that radiation from a single point source emanates radiation uniformly over 4π steradian and this too is dictated by Gauss' flux law and the Divergence Theorem. Such a point source can be described as an infinitesimally small sphere with an infinitesimally small spatial volume, dV or $d\Omega$. This case is analogous to a monopole antenna of very short but finite pole length that shows uniform radiation in all directions covering the full 4π steradian solid angle range; this classic EM simulation can be found in the Remcom technical manual. In contrast to a monopole antenna, an infinitesimally small flat radiation source has an infinitesimally small spatial area, dA it and cannot have dV or $d\Omega$ as its infinitesimal constituent. For this structure, as shown in Fig.3, according to Gauss' flux law in Eq.(2) and Eq.(5), the radiative ray \vec{E} or \vec{D} is ejected orthogonally off the infinitesimal area, dA .

The radiant intensity in the field of wireless communication is meaningfully defined by radiation flux or power contained in a conical volume in space detected from a particular direction. *(This definition will be further justified and elaborated in future publications.)* As such, the radiant intensity quantity detected for a differential-area element in the direction orthogonal to it is the same as the radiant intensity quantity generated by the square area dA , as shown in Fig.3. In physical terms, it is defined as the spatial volume V , of an infinitesimally small differential solid angle $d\Omega$ that contains the total radiant power flux, R , generated by dA . In radio communication, this power density measurement concept is used as a unit to measure the angle-dependent radiant power density that falls over a certain square area in a specific direction given by the direction of a solid angle. This measured power density therefore has a unit of watts per steradian per meter squared ($\text{W}/\text{sr}\cdot\text{m}^2$). This unit is used for measuring the source antenna's radiance and also for approximating the simulated far-field radiation 'gain' pattern, which we shall discuss in latter sections. Here $d\Omega$ is structurally formed by an infinitesimally small azimuthal angle ϕ in the **spherical coordinate system**. In order to find the general equation for radiant intensity emitted by an infinitesimally small flat radiation source, we can proceed to derive the generalized differential solid angle's volume as a function of ϕ . This can be accomplished by making use of spherical coordinates whose variables are ρ , ϕ , and θ . These variables allow us to write the generalized function of radiant intensity by integrating the differential volume $d\Omega$ as shown in Fig.3.

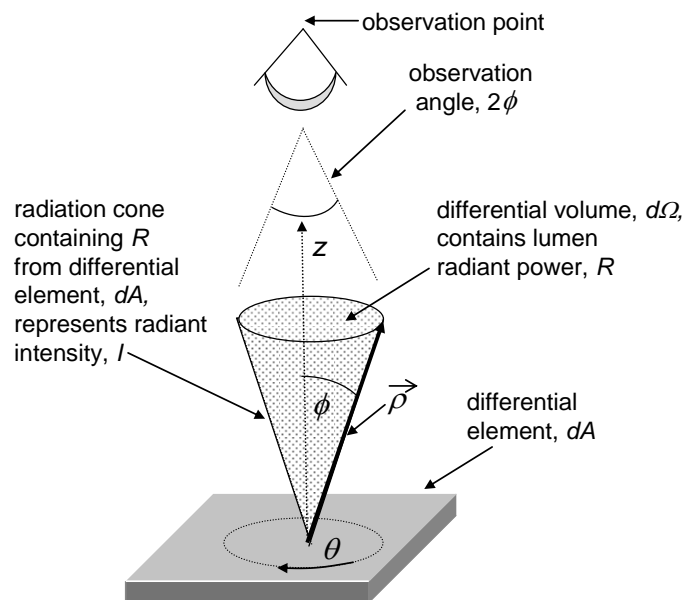


Figure 3. A differential element dA produces its generalized radiant intensity, I , which is the radiant power contained in the radiation cone shown here. The volume of this cone is the integral of $d\Omega$, which is generated by revolving $\vec{\rho}$ over θ in spherical coordinates.

The volume $d\Omega$ contains the radiant power R , where $d\Omega$ is simply created as the vector $\vec{\rho}$, which subtends from the z axis by the azimuthal angle ϕ , and is rotated over θ as θ goes from 0 to 2π .

We can now write the generalized function of radiant intensity for dA as

$$I = (V)(dA)(R) \quad (6)$$

where V is the integral of $d\Omega$. In Eq.(6), V is a unitless numeric quantity as it merely represents the integrated sum value of the differential solid angle (sr) and R has the unit of W/sr-m² since it is the unit radiant intensity per square area, which also known as radiance. Therefore, the unit of I in Eq.(6) is W/sr (not W/sr-m²) which is consistent with the defined unit of radiant intensity, which is a volume intensity inside the cone with generalized parameters such as $\vec{\rho}$ and ϕ . This should not be confused with measured directional area radiant intensity discussed earlier, which is obtained from the volume radiant intensity that falls on a flat surface; thus this ‘area’ radiant intensity will have the unit of W/sr-m². Note that radiant intensity is an unbounded quantity which only when captured by a detector invariably becomes bounded and is then equivalent to radiant intensity per the detector surface area.

It is best to carry out the integral of $d\Omega$ in spherical coordinates as one would use such to calculate the volume of a sphere. For the generalized cone represented by $d\Omega$ in Fig. 3, we note that the length of ρ is arbitrary as is ϕ because we wish to generalize $d\Omega$ as a function of ϕ , but that θ must make a full revolution going from 0 to 2π to form the conical volume. This is a classical problem in advanced calculus that makes use analytic geometry. Utilizing this very approach, we can write the integral of $d\Omega$ as an indefinite volume integral for the ρ and ϕ variables, and a definite integral for the θ variable in (ρ, ϕ, θ) spherical coordinates [15],

$$V = \int_0^{2\pi} \int \int \rho^2 \sin(\phi) d\rho d\phi d\theta \quad . \quad (7)$$

Solving the integral in Eq.(7) leads to

$$V = \frac{2\pi|\rho|^3}{3} \cos(\phi) \quad . \quad (8)$$

where $|\rho|$ is the magnitude of the vector $\vec{\rho}$. Note that a similar mathematical procedure is applied to calculate the volume of a sphere by rotating the V in Eq. (8) to obtain $\frac{4\pi|\rho|^3}{3}$. Inserting Eq.(8) into Eq.(6) leads to the generalized equation for I for a differential-area emitter,

$$I = \frac{2\pi|\rho|^3}{3} (dA) R \cos(\phi) \quad . \quad (9)$$

Since all quantities in Eq.(9) leading to $\cos(\phi)$ are physical constants related to the infinitesimal radiative source dA and the observation or detection distance that relates to $|\rho|$, it can be simplified

as

$$I = C \cos(\phi) \quad (10)$$

where $C = \frac{2\pi|\rho|^3}{3}(dA) R = I_{\max}$, is a constant at a particular observation distance defined by a chosen $|\rho|$.

Eq.(10) is of the form $\rho = b \cos(\phi)$ in (ρ, ϕ) polar coordinates where b is a constant [16]. Eq.(10) is known as the *Lambertian* distribution and is equivalent to Lambert's Cosine Law, which represents the 3D radiant intensity distribution from a flat, differential-area radiation source [8]. Lambert's Cosine Law is widely used and demonstrated in display science and technologies as they utilize flat display panels and these too generate light or EMR radiation in space according to Lambertian distributions. It is important to note while Lambert's Cosine Law does not specify the constant, C , our derived Eq.(10) actually provides it exactly. Further, our method of deriving Eq.(10) using Maxwell's Equations and Gauss' Divergence Theorem is consistent with what Lambert discovered in the eighteenth century, which is a very intriguing result. Our analytic formula for near-field radiation intensity, consistent with Lambert's law, holds for a finite flat radiator, which is the most basic, practical element for a wireless and cellular antenna.

Although the EMR spatial distribution is routinely demonstrated to show a Lambertian distribution for a flat optical radiator, it is important to go through the above mathematical physics exercise in spherical coordinates to see how such a distribution forms. This very exercise allows one to analytically determine the EMR distribution for a finite size flat antenna patch, which is presented next.

In order to determine the near-field radiant intensity distribution for a finite-size patch antenna, we consider the radiation emitting surface in Fig.2 to be a single layer that is mathematically represented by adding many dA 's over the total area equaling $X_L Y_L$. This layer, when sufficiently thick, can be represented as an aggregate of many sandwiched layers where each layer can contain many radiative elements. For simplicity, here we consider one aggregate layer as the radiation emitting surface.

Supposing there are $m \times n$ dA 's for the radiation emitting surface as shown in Fig.2, then each dA would generate a $d\Omega$ as shown in Fig.3, and the total radiant intensity for this finite patch antenna can be obtained by integrating all the $d\Omega$'s over the area, $X_L Y_L$. Here we assume that each radiative element generates an inherent radiance R_{avg} and that all such elements are uniformly distributed over the active antenna structure. For thick layers comprising ' i ' number of layers where each layer has ' $m \times n$ ' radiative elements, we can represent that case via multiplying ' $m \times n$ ' by ' i '. For simplicity, we omit this multiplier ' i ' for radiance, R_{avg} .

For a highly efficient antenna patch, ' $m \times n$ ' is very large and in that case many of these differential cones, $d\Omega$'s would be overlapping as shown on the left side in Fig.4.

In the limit where ' $m \times n$ ' or simply ' mn ' is very large and because $d\Omega$ is infinitesimally small, the entire patch antenna would be filled with very small radiative elements with each cone essentially overlapped by many others. The aggregate radiant intensity for the finite patch antenna, PA , then becomes,

$$I_{PA} = (mn) R_{avg} X_L Y_L (V) \quad (11)$$

where V , the volume of $d\Omega$, is given by Eq.(8).

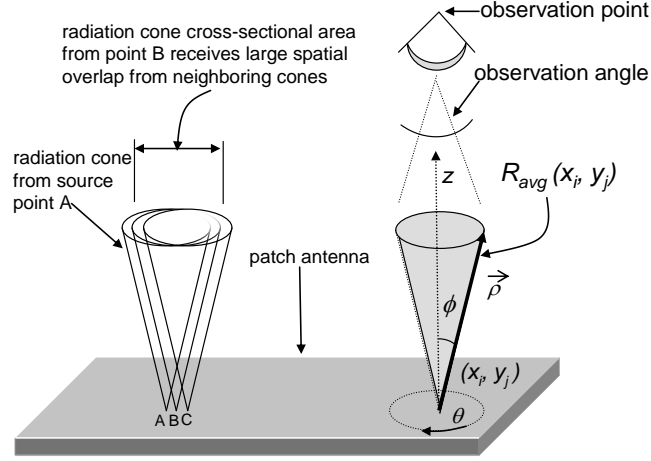


Figure 4. A schematic diagram depicting average radiance R_{avg} from a radiative element at location (x_i, y_i) in the bounded volumetric cone shown at the right side of a patch antenna. On the left side, the large overlap of radiance from points A, B, and C are shown as $d\Omega$'s are substantially overlapped.

Therefore, we obtain,

$$I_{PA} = \frac{2\pi|\rho|^3}{3} (mn) R_{avg} X_L Y_L \cos(\phi) \quad (12)$$

In Eq.(11) and Eq.(12), R_{avg} is the average radiance over the flat antenna that is used for the entire surface antenna since in reality, radiance per each small surface area could be slightly different due to uniformity of the antenna's material properties. As before, since all quantities leading to $\cos(\phi)$ are physical constants related to the patch antenna, it can be simplified as

$$I_{PA} = C_{PA} \cos(\phi) \quad (13)$$

where $C_{PA} = \frac{2\pi|\rho|^3}{3} (mn) R_{avg} X_L Y_L$, is again a constant at a particular observation distance defined by a chosen $|\rho|$.

Eq.(12) describes the 3D radiation intensity generated by the single patch antenna off its surface, which is equivalent to Ψ_0^2 in Eq.(1). It is not the transverse (2D) field intensity on the surface of the antenna whose power would be measured in W/m^2 ; but rather the 3D radiation intensity observed or detected by a viewer from particular angle ϕ and measured using units of $\text{W}/\text{sr}/\text{m}^2$. The measurement unit relations between $\text{W}/\text{sr}/\text{m}^2$ and W/sr have been explained previously. **Because Eqs.(12) and (13) occurs at time, $t = 0$ and it represents intensity, there is no time or temporal frequency dependence in these equations.**

Eq.(13) is a function that describes a Lambertian in polar coordinates where C_{PA} is a factor containing constant parameters relating to the patch antenna and the chosen detection distance; and the magnitude of I_{PA} varies according to $\cos(\phi)$. As ϕ spans from $-\pi$ to $+\pi$ steradian, I_{PA} forms a 3D Lambertian distribution in space. Therefore, Eq.(13) is the 3D Lambertian a finite-size patch antenna produces for its radiant intensity distribution. It is important to note that when $\vec{\rho}$ has a particular finite length that produces one unit of radiant intensity within 1 unit of solid angle bounded by 1 unit of square area in a particular unit system, Eq.(13) represents the radiance distribution for the patch antenna in 3D, which can be measured directly using 3D radiation detection techniques. By measuring the radiance distribution and the total radiation power flux an antenna emits, the radiation intensity distribution can be experimentally determined using Eq.(13) in near-field. This has been experimentally demonstrated in the field of display and lighting at optical frequencies [7]. Similarly radiant intensities can be measured for RF frequencies and one would expect similar Lambertian type distributions for antennas as well.

Our derivation of Eq.(13) is a closed-form analytic solution of the radiant intensity distribution for a finite, flat radiating antenna that is related to its gain function. It is achieved only using basic Maxwell's equations and Gauss' Divergence Theorem and without having to solve the wave equation. It is an important contribution because here **we have a closed-form equation for the radiant intensity in 3D near field that relates to the size of the antenna as well as its inherent quantum efficiency**, which involves taking the input RF power and converting it to the wireless antenna radiance. The radiance of an antenna is its inherent characteristic. Such an equation is helpful in figuring out how to improve and optimize the inherent quantum efficiency of a basic flat antenna element, which can lead to higher antenna gain.

Although we have made simplified assumptions that all mn radiative elements have the same radiance R_{avg} , and that they are uniformly distributed over the active patch antenna, the above analysis can still be carried out for separate local regions of locally uniform radiance of radiative elements and adding the equivalent of Eq.(10) for each region. The additions of several separate sums will again produce another cosine relationship because one would be adding two or more cosines. It is important to note that since we have not incorporated any time-dependent phenomenon in this analysis, Eq.(13) represents the instantaneous radiant intensity distribution of a finite patch antenna and this is different from the steady state case.

We can generalize Eq.(13) for further benefit towards calculating the radiation pattern and directivity for flat antennas. The generalized form of this equation in ρ - ϕ polar coordinates is known as a 'cardioid' and can be written as,

$$\rho = a + b \cos(\phi) \quad (14)$$

where ‘ a ’ and ‘ b ’ are constants, representing shift and weighting parameters respectively. This is also the directivity equation, which we shall discuss further in Section 3. When $a = 0$, we get a Lambertian radiation pattern where b is the maximum value of ρ that occurs at $\phi = 0$.

We have derived an analytic formula that describes the near-field radiation intensity pattern of a finite-size patch antenna. We have shown that a flat antenna produces a Lambertian intensity distribution in near-field in 3 dimensions and it in fact looks like a sphere. This simple formula, however, is very **complicated** to visualize in 3D. Its spherical boundary does not represent equal radiant intensity on its spherical surface! This mistake is often made because many find it difficult to recognize the placement of this sphere with respect to the origin of a spherical coordinate system.

A 3D Lambertian is difficult to depict on a plane and as such, only a slice from this 3D Lambertian is typically drawn [8], which represents the intensity distribution on a specific plane, i.e., xz or yz planes in a Cartesian coordinate system. However, with the right graphing tool, one can plot the whole 3D Lambertian intensity profile using false colors. Therefore, we present the graph of Eq. (13) in Fig. 5 using false colors to represent the varying radiant intensity values.

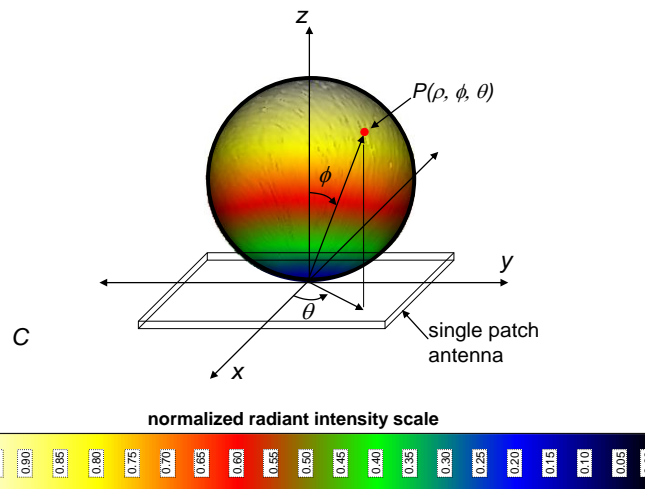


Figure 5. The near field 3D radiation pattern from a single-patch flat antenna calculated using the derived analytical equation in Eq.(13). The normalized radiant intensity is plotted in spherical coordinates by sweeping $\bar{\rho}$ as ϕ spans from $-\pi$ to π and θ from 0 to 2π .

The pattern in Fig.5 is a Lambertian distribution where the peak radiation intensity occurs at the center of the patch. The perimeter of Lambertian sphere and the peak intensity increase with increasing R_{avg} , X_L and Y_L . The color map in the figure provides the intensity variation showing a cosine falloff as ϕ increases for any θ ranging from 0 to 2π .

Currently, many simulation tools only calculate the near field 2D electric field or current distribution on the radiative source surface, but do not calculate the near-field 3D radiation pattern. Instead, they calculate the far-field 3D radiation pattern by propagating the 2D near-field sufficiently far away to approximate the power gain function that provides the EMR power density

distribution in far-field. However, such an approximation is not very useful or accurate, and in most cases designers resort to approximating the EMR power density at a particular location by physical measurements often assuming some incorrect density uniformity and comparison methods. Such approaches fail to provide a good understanding of how a radiation source produces EMR in space in a directional manner and how it is carried along in space as it propagates through real distances. Physical measurements even when absorption and scattering are absent in the environment are often inaccurate because the EMR spatial distribution from flat antennas is substantially non-uniform by nature. *The actual degree of this non-uniformity is very important.*

Since the simulation of a 3D near-field EMR distribution from a flat patch antenna is not available to us at this time, we validate our result presented in Fig.5 qualitatively by studying the simulated far-field EMR energy distribution from a single patch antenna. For this comparison, we use Remcom's [17] finite-difference time-domain (FDTD) software to simulate the far-field radiation intensity pattern and propagate it backwards using its directivity properties to represent the 3D near-field radiation intensity distribution. In Fig.6, we plot the simulated results from a small patch antenna and note the similarity with that from Fig.5. The far-field or near-field radiation intensity simulations, which scales with the power gain simulation, shown in Fig.6 do not have any time dependent factors for the same reasons we do not have time dependent factors in Eqs.(11), (12), and (13). For intensity calculations ($I \propto \vec{E} \cdot \vec{E}^*$ or $I = |\vec{E}|^2$), $e^{-j\omega t}$ simply drops out.

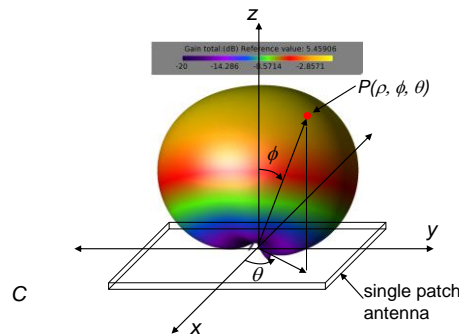


Figure 6. The near field 3D radiation intensity pattern from a single patch antenna simulated using the electromagnetic software from Remcom. The radiant intensity is plotted in spherical coordinates by sweeping $\vec{\rho}$ as ϕ spans from 0 to 2π and also θ from 0 to 2π . The color codes of this plot are the same as that in Figure 5.

In the simulation, a single patch antenna is fed by means of a sinusoidal voltage source at 28 GHz with 50Ω impedance. The patch size is 3.405mm X 3.405mm, which sits on a dielectric substrate of size 15mm X 15mm X 0.254mm; the dielectric substrate is placed above the ground plane (15mm X 15mm) and provides electrical isolation between the patch and ground. The voltage source, represented by a single circuit component, is placed between the patch antenna and ground, near the center of antenna. Since the source impedance does not have an ideal match with that of

the patch antenna, a small reflection is produced at the center of the patch. Fig.6 shows the simulated near-field radiation pattern resembling a Lambertian distribution perturbed by some reflection waves just above the center of the antenna where it is fed. The resemblance between Figs.5 and Fig. 6 validates our near-field analytic solution. Since a Lambertian distribution (strictly a cosine distribution) is produced in near field from a flat radiation source as seen in Fig.5, the far-field of this radiation is also expected to be a Lambertian or a cosine distribution. This is true because one can take the Fourier Transform of the near field spatial intensity **in the spatial domain rather than in the time domain**. Doing so yields that Fourier Transform of a cosine is also a cosine, ensuring that spatial propagation covering all space guarantees that a cosine spatial distribution always remains a cosine. {The discipline that covers Fourier Transforms in the spatial domain is better known as Fourier Optics, which is an established field in optics. Nevertheless, the same mathematics applies to the spatial characteristics of microwave radiation [18] or radiation at any frequency.} It is important to note that the far field radiation is a broadened Lambertian (a cosine scaled differently from the near-field) compared to that of the near-field due to wave propagation over a very long distance. In the next section we analyze how a Lambertian radiation and its 2D projection along wavefronts broaden as it propagates in space. We do so by deriving the 2D projection of the 3D Lambertian intensity pattern on the surface of the antenna.

3. Derivation of the 2D Near-field Power Density Distribution and Radiation Propagation Equation of a Flat Antenna

A. Derivation of the 2D Near-Field Power Density Profile of a Single Patch Antenna

In the previous section, we derived the near-field EMR power density distribution in 3D space for a single patch antenna of a certain size. Here we derive the 2D surface power density on the antenna surface by simply taking the projection of this 3D radiation pattern on to the surface of the single patch antenna!

The projection of the 3D Lambertian function in Eq.(14) when $a = 0$, on to the surface of the flat antenna can be achieved by making use of both ρ - ϕ polar coordinate and ρ - ϕ - θ spherical coordinate systems. In Fig.5, we note that all points representing the radiant intensity from a flat antenna is given by P that is described by the vector $\vec{\rho}$. The radiation pattern is fully defined for a flat antenna by $\vec{\rho}$ where it is maximum at the center of the flat antenna; and for all other points, $P(\rho, \phi, \theta)$ on the radiation pattern of the antenna is defined by varying $\vec{\rho}$ according to Eq.(14) for various ϕ and θ . In order to find the projection of this Lambertian on to the surface of the patch antenna, we need to determine the projections of all its points $P(\rho, \phi, \theta)$ on the xy plane. We do so by first representing the polar vector $\vec{\rho}$ that extends to any point P on the Lambertian pattern. i.e., $P(\rho, \phi)$, in 3-variable spherical $[P(\rho, \phi, \theta)]$, cylindrical $[P(r, \theta, z)]$, and Cartesian $[P(x, y, z)]$ coordinate systems. The procedure involves utilization of transformation among spherical, cylindrical and Cartesian coordinates. We then determine the projection of $P(x, y, z)$ onto the xy plane, which is $P'(x, y, \theta)$. Finally, the surface intensity can be found by determining the corresponding z [magnitude of P' at (x, y)] values for each $P'(x, y)$.

The problem of determining the surface intensity from the projection of the 3D radiation intensity has been solved in **detail previously** [7]. Therefore, here we omit the details and only highlight the main transformation equations applied to derive the equation that lets us calculate z for

all $P'(x,y)$ on the antenna surface. The well-known transformation relations among spherical, cylindrical and Cartesian coordinate systems are [19]:

$$x = \rho \sin(\phi) \cos(\theta), y = \rho \sin(\phi) \sin(\theta), z = \rho \cos(\phi), \quad \text{and, } x^2 + y^2 + z^2 = \rho^2 . \quad (15)$$

Using the relations in Eq.(15), we can find all projected locations $P'(x,y,0)$ of $P(\rho,\phi,\theta)$ and their corresponding z values. We do so by varying ϕ from $-\pi$ to π , and θ from 0 to 2π and determine the corresponding x , y , and z values using Eq.(15). Noting that z is only dependent on ϕ and therefore for a particular ϕ and any θ , the value of z is simply $z = \rho \cos(\phi)$; in other words, the graph of I_{PA} projected on the xy plane is simply given by $z = \rho \cos(\phi)$. We plot this 2D surface intensity graph in Fig. 7 where the value of C_{PA} is taken to be 1.

Fig.7 shows the projection of the 3D Lambertian from Fig.5 on the xy plane and it is therefore the 2D surface intensity profile for a finite, flat or patch antenna such as that shown in Fig.5 under the Lambertian distribution. This projection on the xy plane is obtained for all points $P(\rho, \phi, \theta)$ of the 3D Lambertian described by Eq.(13) and each such point on the xy plane corresponds to a z value determined from the relations in Eq.(15). These z values represent the surface intensities at (x,y) on the xy plane.

Essentially, then, the xy projection is a graph of some function, $F(x,y) = z$ where all points of this function are represented by the projected points $P'(x,y,0)$ of $P(\rho, \phi, \theta)$ and $P(r, \theta, \phi)$. We note that the projection of I_{PA} on the xy plane is a paraboloid in (r, θ, z) cylindrical coordinates that is described by [20],

$$z = C_{PA} - r^2 \quad (16)$$

where, $r^2 = x^2 + y^2$ and x , y , and z are specified according to Eq.(15); and z has a ϕ dependence, where ϕ is azimuthal angle variable in spherical coordinates.

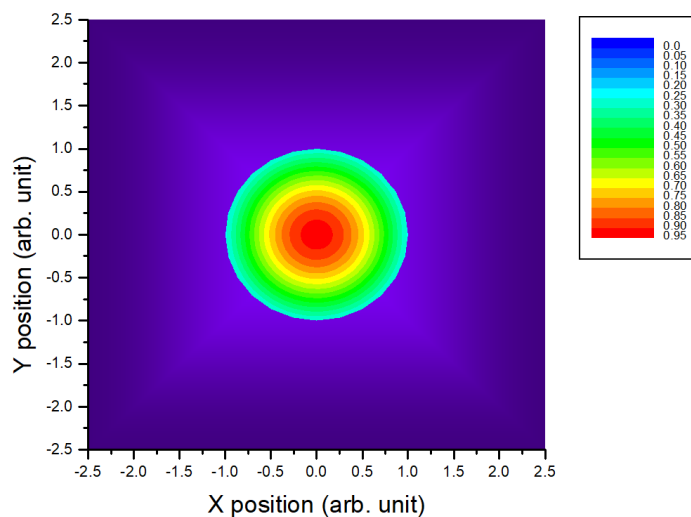


Figure 7. The 2D surface intensity profile from a single patch flat antenna calculated by projecting the graph in Fig.5 onto the xy plane. The normalized surface intensity is plotted from the projection of \bar{P} as ϕ spans from $-\pi$ to π and θ from 0 to 2π .

Fig. 7 is consistent with Eq.(16) and indeed shows the concentric circular profiles that describe the surface intensity of a square, flat, radiating source. The 3D version of the surface plot in Fig.7 is indeed a paraboloid, which we shall see in the following sub-section.

In order to qualitatively validate our derived 2D surface intensity profile of a flat conductor, we again use Remcom’s electromagnetic simulation software. Because some artifact that invariably gets generated due to discrete gridding in symmetric structures, here we present two simulated results to compare against our analytic results. The first simulated result is presented in Fig. 8(a), which shows the near-field electric field flux distribution (i.e., $|E|$) over a finite-size patch antenna) of the same patch antenna whose 3D radiation intensity pattern, is shown in Fig.6. This structure was fed asymmetrically in order to avoid the power cancellation that would otherwise occur in the symmetric case in the particular finite and discrete simulation method we used here. Fig.8 (a) shows concentric and nearly circular contours of electric field flux on the flat antenna surface, where the maximum value occurs at the center of the patch as expected. The aberrations in the concentric contours that deviate from perfect circles are due to the asymmetric feed intentionally provided to the patch antenna. In order to validate that one actually obtains perfectly circular contours on the surface, in Fig. 8(b), we present the electric field distribution on a flat conductor that is fed symmetrically with the same voltage source from the same sinusoidal 50Ω RF generator at 28 GHz. In Fig.8(b), we see similar concentric circular patterns as those depicted in Fig.7. Although Fig.7 plots the surface intensity, its corresponding electric field flux distribution (i.e., $|E|$) will also have this distribution profile, described by concentric circles where the maximum would occur at the center because $I \propto \vec{E} \cdot \vec{E}^*$.

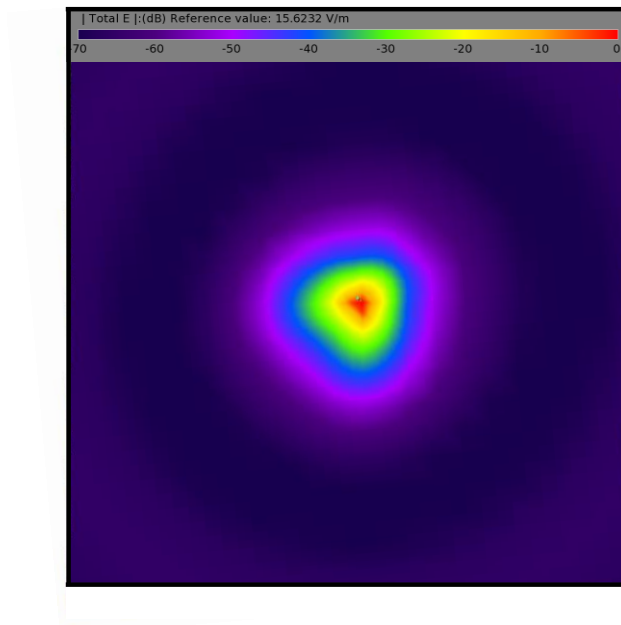


Figure 8(a). The simulated 2D surface electric field flux profile of the single patch antenna for which we presented the 3D radiation intensity simulation in Fig.6. Both simulations are performed using the Remcom software. An asymmetric or an off-centered feed was intentionally used for this simulation.

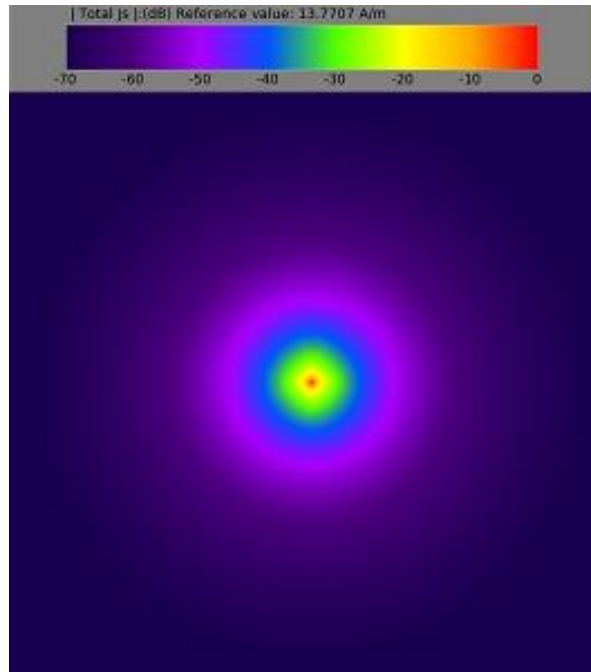


Figure 8(b). The 2D surface electric field flux profile of a flat conductor simulated using the Remcom EM software where we have used a symmetric feed that was placed at the center of the radiator.

Fig. 8(b) shows concentric circular profiles for the surface electric field flux and this is what we would expect since the magnitude of the electric field flux is proportional to the square root of the radiant intensity, I_{PA} .

It is important to note that our comparison between Fig.7 and the two figures, i.e., Fig.8(a) and Fig.8(b), are qualitative only as Fig.7 represents the instantaneous surface intensity profile of an flat antenna of an arbitrary size where as Figs.8 provide the steady-state surface electric field flux profiles of a flat conductor of a specific size at a single operating frequency. We also note that the magnitudes of the concentric contours in Figs. 8(a) and 8(b) near the edge of the conductor do not decrease at the same rate as those seen in Fig.7. This is primarily due to the fact that our analytic formula represents the instantaneous intensity where as the results plotted in Figs.8(a) and 8(b) represent the steady-state field flux. While the instantaneous solution produces a paraboloid for the surface intensity distribution of a flat antenna, the steady-state solution would produce a Gaussian-like field distribution on the antenna surface showing the rise and fall time effects at the edges of a paraboloid. Nevertheless, the perfect circular contours on the surface seen in Fig. 7 and Fig. 8(b) provides a good qualitative validation that a 3D Lambertian radiation pattern produces a Gaussian-like field distributions on the antenna surface. The Gaussian-like field distribution pattern can be thought of as a paraboloid modified by means of rise and fall time effects. Although we are unable to provide here an experimental comparison of Fig.7 due to the complexity involved in measuring the near-field intensity of a mm-size antenna, we have experimentally verified its equivalence for and optical radiator previously [7].

B. Derivation of the Radiation Propagation Equation from a Single Patch Antenna

In Section 2, we derived the closed form analytic solution for the instantaneous intensity distribution on a flat radiating conductor or patch antenna. It is a closed form solution because C_{PA} is entirely defined by the patch antenna's x and y dimensions as well as its inherent radiance of each radiative element. The value of $|\rho|$ in Eq.(13) takes on a definite value when the radiance distribution is measured for the antenna using a particular measurement unit, such as the *SI* unit of $W/sr\text{-m}^2$. If C_{PA} is determined using the *SI* unit, $|r|$ and z in Eq.(16) would be some length or distance variable represented in meters. Note that while C_{PA} would be determined from Eq.(13), which include $|\rho|$ that comes from utilizing the (ρ, ϕ, θ) spherical coordinate system, r is a variable defined in the cylindrical coordinate system.

Eq.(16) is a function in space that is described by $f(z) \propto r^2$. In order to derive the radiation propagation equation for a patch antenna, it is most suitable to use Eq.(16) and utilize a coordinate system that uses the variables ρ , ϕ , and z because from ρ , one can determine r by taking its projection onto the xy plane. In this coordinate system, the EMR's conical spreading zone is represented by vector $\vec{\rho}$, which is related to the azimuthal direction, z , by angle ϕ . The azimuthal direction, z , is the propagation axis for radiation emitted by flat antennas. The ρ - ϕ - z coordinate system is known as the cylindrical coordinate system and it is used below in all formulations hereafter. The same coordinate system is also used by others in beam propagation [21].

The beam propagation of the surface intensity described by Eq.(16) can be fairly easily obtained since it is the source beam profile at $z = 0$. From this beam intensity profile we can determine the transverse electric field flux distribution, $\Psi(x, y, z)$. Following the arguments used in [20], the transverse field flux distribution for the patch antenna described in Fig. 2 at some distance z along this propagation axis is given by the electromagnetic wave, Ψ ,

$$\Psi(x, y, z) = \Psi(x, y, 0) e^{\pm j\vec{k} \cdot \vec{\rho}} \quad (17)$$

where $\Psi(x, y, z)$ is the surface electric field distribution at z , \vec{k} is given by $\vec{k} = \frac{2\pi}{\lambda} \sqrt{\vec{\mu} \times \vec{\varepsilon}}$ and $\rho = \sqrt{x^2 + y^2 + z^2}$, where μ and ε are propagation medium's permeability and permittivity respectively. Assuming the paraboloid beam propagates in the forward z direction in a homogeneous medium where the impedance, $\eta = \sqrt{\mu/\varepsilon}$ is constant in space, Eq.(17) can be simplified as

$$\Psi(x, y, z) = \Psi(x, y, 0) e^{-jk\rho} \quad (18)$$

where ρ and z are related by $z = \rho \cos(\phi)$.

Here we note that at $z = 0$, $\Psi(x, y, 0) = \Psi_0 = \sqrt{C_{PA} - r^2} = \sqrt{C_{PA} - (x^2 + y^2)}$.

As Ψ_0 propagates along z , its phase " $jk\rho$ " oscillates as $e^{-jk|\rho|}$ and Ψ at z broadens according to the projection of $\vec{\rho}$ on the source plane represented by the vector \vec{r} at the point (r, θ) . As the propagating wave vector $\vec{\rho}$ gets larger with increasing z , the vector \vec{r} on the xy plane at $z = 0$ now spreads over a larger radius r where $r^2 = x^2 + y^2$ as seen in Fig.9.

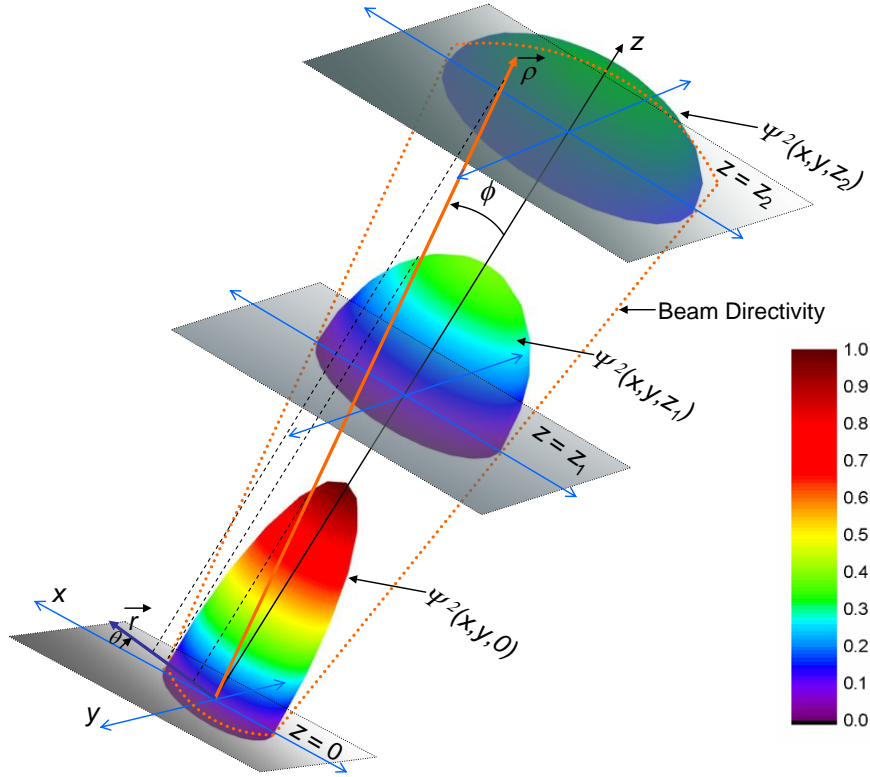


Figure 9. The propagation of antenna surface intensity distribution, Ψ^2 , along the propagation axis, z . The surface intensity distributions at $z = 0, z_1$, and z_2 are calculated using our derived formula and shown here as 3D surface plots using the colormap scale shown on the right. This figure shows the geometric relation between $\bar{\rho}$ and \bar{r} , which must be distinguished carefully. The beam directivity is shown in orange dotted lines. The peak values of the paraboloids at z_1 and z_2 drop to 50% and 25% respectively of the maximum peak value at $z=0$.

Fig. 9 clearly shows that a flat antenna EMR is a beam that propagates along the center propagation axis, z . As this EMR radiation beam propagates farther, the peak of Ψ along z , where $x=y=0$ and $\rho = z$, will lose strength as $C_{PA} - (x^2 + y^2)$, because as z increases, so does $(x^2 + y^2)$ according to larger $\bar{\rho}$ and \bar{r} . The calculated xy surface distribution profiles of $|\Psi|^2$ at $z = 0, z_1$ and z_2 are shown in Fig. 9 based on our derived formulas in Section 3A. The full transverse (x,y) distributions of $|\Psi|^2$, i.e., the surface intensity distributions at various z in Fig. 9 are paraboloids of diminishing peak values with increasing z .

In Fig. 9, $|\Psi_0|^2$ at $z = 0$ is the same profile as that presented in Fig. 7. In Fig.9 we show the 3D surface plot, whereas in Fig.7, we show its corresponding contour plot. The analysis presented here by means of Fig.9 demonstrate that our derived analytic formulas for the near-field 3D and 2D intensity distributions of a finite-size patch antenna allow one to determine how the beam generated by the antenna propagates in space. Such analysis provides a method to calculate the power density from a single patch antenna at any point in space.

Although we have only focused on the spatial part of the EM wave in our derivations, we note that we can easily incorporate time dependence in the EM radiation field flux E given by Eq.(1), by carrying along the term $e^{-j\omega t}$ for a flat, patch antenna. It is most important to first find the flux distribution Ψ_0 , which then gives flux distribution for all $|\bar{E}|$ over the X_L by Y_L area, since $I \propto \bar{E} \cdot \bar{E}^*$

or $I = |\bar{E}|^2$. We can then easily update Eqs. (11), (12), (13), (16), (17) and (18) by adding the time varying term $e^{j\omega t}$ to derive the field distribution at any point in space and time. Such an extension will also help us derive the analytic equations for the steady state case that is reached after some transient period. These will represent the time-averaged amplitudes and intensities for antennas.

7. Conclusions

Wireless communications using mm-Wave frequencies are now globally used among general population. We can expect the number of subscribers or endpoints to substantially increase along with service upgrades that require substantially higher bandwidth. As such, 5G systems are now currently considered as well as deployed for which it is very important that we accurately predict the required signal power densities at certain locations. Since 5G utilizes higher carrier frequencies than those used in previous generations, it needs higher power per frequency channel, leading to much higher overall power densities in space. The affects of going to higher frequency is that the EM wave signal will experience higher attenuation when it goes through material; diffraction of waves will incur higher attenuation; and reflection and scattering will also be problematic at higher frequencies. These effects have affected recent measurements [22] [23] [24] that indicate very sharp decorrelation over small distance movements of just a few tens of wavelengths at mm-Wave, depending on antenna orientation. It is therefore crucial that we first have some accurate means of determining the basic and uninterrupted spatial power density distributions generated from 5G antennas and our equations combined with our simulation tools allow us to obtain them. Failing to know the accurate spatial power density distributions at the source antenna could result in inefficient usage of power and too much RF power density can also have safety concerns. In order to gain a foothold on only generating a sufficient power density distribution at the antenna surface and to not exceed the peak power density beyond a certain point, our derived formulas can be used to ensure that peak power density from a flat antenna source stays as limited as necessary.

Here we have presented a novel derivation of the 3D near-field radiation intensity of a finite, flat radiation source, which is the basic antenna element used in many wireless systems. The approach allowed us to derive the analytic formula for the surface intensity, which plays a core part in determining how the beam from flat antennas radiates in space. Our formulas and analysis provide the means to calculate the power density on any surface at any location that is some arbitrary distance away from the source antenna. We validated our analytic solutions to a good and understandable extent using the Remcom EM simulation software albeit some small mismatches that are expected due to a number of conditions that include both real effects as well as artifacts. Our closed-form solutions can be utilized to predict the peak and minimum power densities generated by flat antennas of certain sizes and input power. Further, in the future, we can combine our analytic tools with an EM software tool such as Remcom or other, to calibrate realistic designs of patch antennas producing optimized power gain that can be quite effective for 5G and other wireless systems. Our future work will include extending our formulas to incorporate rise and fall time effects for single patch as well as 2D patch antenna arrays that operate in coherent and incoherent conditions, which we can comprehensively validate using the patch array simulations that have already been achieved [25]. Finally, our work will revolutionize the near-field radiometry and photometry industries in simplifying the substantial complexities associated with such measurements and analysis.

References

- [1] T. S. Rappaport et al., “Millimeter wave mobile communications for 5G cellular: It will work!” *IEEE Access*, vol. 1, pp. 335–349, May 2013.
- [2] A. Ghosh et al., “Millimeter-wave enhanced local area systems: A high data-rate approach for future wireless networks,” *IEEE J. Sel. Areas Commun.*, vol. 32, no. 6, pp. 1152–1163, Jun. 2014.
- [3] W. Roh et al., “Millimeter-wave beamforming as an enabling technology for 5G cellular communications: Theoretical feasibility and prototype results,” *IEEE Commun. Mag.*, vol. 52, no. 2, pp. 106–113, Feb. 2014.
- [4] 5GCM, “5G channel model for bands up to 100 GHz,” Tech. Rep., Oct. 2016. [Online]. Available: <http://www.5gworkshops.com/5GCM.html>.
- [5] K. Haneda et al., “Indoor 5G 3GPP-like channel models for office and shopping mall environments,” in *Proc. IEEE Int. Conf. Commun. Workshops (ICC)*, May 2016, pp. 694–699.
- [6] S. Deng, M. K. Samimi, and T. S. Rappaport, “28 GHz and 73 GHz millimeter-wave indoor propagation measurements and path loss models,” in *Proc. IEEE Int. Conf. Commun. Workshop (ICCW)*, Jun. 2015, pp. 1244–1250.
- [7] M. Nisa Khan, “Derivation and Experimental Verification of of the Near-field 2D and 3D Optical Intensities from a Finite-size Light Emitting Diode (LED),” *IEEE Photonics Journal*, 11(6), December 2019.
- [8] https://en.wikipedia.org/wiki/Lambert%27s_cosine_law, Accessed on February, 2022.
- [9] M. K. Samimi, T. S. Rappaport, and G. R. MacCartney, Jr., “Probabilistic omnidirectional path loss models for millimeter-wave outdoor communications,” *IEEE Wireless Commun. Lett.*, vol. 4, no. 4, pp. 357–360, Aug. 2015.
- [10] M. K. Samimi and T. S. Rappaport, “3-D millimeter-wave statistical channel model for 5G wireless system design,” *IEEE Trans. Microw. Theory Techn.*, vol. 64, no. 7, pp. 2207–2225, Jul. 2016.
- [11] S. Sun, H. Yan, G. R. MacCartney, Jr., and T. S. Rappaport, “Millimeter wave small-scale spatial statistics in an urban microcell scenario,” in *Proc. IEEE Int. Conf. Commun. (ICC)*, May 2017, pp. 1–7.
- [12] S. Ramo, J. R. Whinnery, and T. Van Duzer, *Fields and Waves in Communication Electronics*. New York, Wiley, 1965, pp. 135-137.
- [13] S. Ramo, J. R. Whinnery, and T. Van Duzer, *Fields and Waves in Communication Electronics*. New York, Wiley, 1965, Chapters 1-3.
- [14] J. D. Jackson, “Classical Electrodynamics”, John Wiley & Sons, New York, 1975, Chapter 1, Section 1.3, “Gauss’ Law”, pp. 30-33.
- [15] E.W. Swokoski, "Calculus with Analytic Geometry", 2nd Edition, Prindle, Weber, and Schmidt, Boston, Massachusetts, 1981, pg. 875, Chapter 17.
- [16] E.W. Swokoski, "Calculus with Analytic Geometry", 2nd Edition, Prindle, Weber, and Schmidt, Boston, Massachusetts, 1981, pg. 635, Chapter 13.
- [17] <https://www.remcom.com/> Accessed on February, 2022.
- [18] Joseph W. Goodman, “Introduction to Fourier Optics”, Roberts and Company Publishers; 3rd Edition (December, 2004).
- [19] E.W. Swokoski, "Calculus with Analytic Geometry", 2nd Edition, Prindle, Weber, and Schmidt, Boston, Massachusetts, 1981, pg. 712, Chapter 14.
- [20] E.W. Swokoski, "Calculus with Analytic Geometry", 2nd Edition, Prindle, Weber, and Schmidt, Boston, Massachusetts, 1981, pg. 802, Chapter 16.
- [21] S. Ramo, J. R. Whinnery, and T. Van Duzer, *Fields and Waves in Communication Electronics*. New York, Wiley, 1965, Chapters 3, pg.160.
- [22] T. S. Rappaport, G. R. MacCartney, Jr., S. Sun, H. Yan, and S. Deng, “Small-scale, local area, and transitional millimeter wave propagation for 5G communications,” *IEEE Trans. Antennas Propag.*, vol. 65, no. 12, pt. I, pp. 6474–6490, Dec. 2017.
- [23] M. Rumney, “Testing 5G: Time to throw away the cables,” *Microw. J.*, Nov. 2016, pp. 10–18.
- [24] M. K. Samimi and T. S. Rappaport, “Local multipath model parameters for generating 5G millimeter-wave 3GPP-like channel impulse response,” in *Proc. 10th Eur. Conf. Antennas Propag. (EuCAP)*, Apr. 2016, pp. 1–5.
- [25] Scott Langdon, “Using CDF to Access 5G Antenna Directionality”, Invited Paper, *Microwave Journal*, August 2019.